Mon. Not. R. Astron. Soc. **000**, 1–14 (2004) Printed 5 February 2008 (MN LATEX style file v2.2)

Beppo-SAX temperature maps of galaxy clusters in the Corona Borealis supercluster: A2061, A2067 and A2124

F. Marini[1], S. Bardelli [1],⋆ E. Zucca[1],⋆ S. De Grandi[2], A. Cappi[1], S. Ettori [3], L. Moscardini [4], G. Tormen [5], A. Diaferio[6]

[1] *INAF - Osservatorio Astronomico di Bologna via Ranzani 1, I–40127 Bologna, Italy*
[2] *INAF - Osservatorio Astronomico di Brera, via Bianchi 46, I–23807 Merate (LC), Italy*
[3] *ESO - Karl-Schwarzschild Strasse 2, D–85748 Garching, Germany*
[4] *Dipartimento di Astronomia, via Ranzani 1, I–40127 Bologna, Italy*
[5] *Dipartimento di Astronomia, vicolo dell'Osservatorio 2, I–35122 Padova, Italy*
[6] *Dipartimento di Fisica Generale "A. Avogadro", via Giuria 1, I–10125 Torino, Italy*

Accepted 00-00-0000, Received 00-00-0000 in original form

ABSTRACT

In this paper we present the analysis of Beppo-SAX observations of the cluster pairs A2061–A2067 and A2122–A2124, located in the Corona Borealis supercluster, which have been selected as candidate merging clusters. The aim of this work is to study the physics of the intracluster medium and to look for the possible presence of merging signatures. We derived the global temperatures and abundances and the temperature profiles and maps for these clusters. We do not find any significant evidence of interaction between the clusters forming the pairs, but we detect a candidate shock inside A2061. On the basis of the X-ray and optical properties of this cluster we propose a scenario in which a group is falling inside A2061. This interaction is in the phase in which the cores have not encountered yet and in which the formation of a shock is expected.

Key words: X-rays: galaxies: clusters - galaxies: clusters: general - galaxies: clusters: individual: A2061 - galaxies: clusters: individual: A2067 - galaxies: clusters: individual: A2122 - galaxies: clusters: individual: A2124 -

1 INTRODUCTION

Clusters of galaxies are by now recognized to form in a hierarchical way, by the gravitational merger of smaller clusters and groups. This kind of events are the most energetic ones in the Universe since the Big Bang, with a release of $\sim 10^{50} - 10^{60}$ erg on a time scale of the order of few Gyrs (Sarazin 2000).

Numerical simulations (Tormen 1997) revealed that mergings happen along preferential directions which define matter flow regions, at whose intersection rich clusters form. The environment of these intersections is represented by the core of superclusters: given the high local density and the small volumes involved, the "cross section" for merging between clusters or group-cluster is strongly enhanced and the dynamical processes are accelerated. Therefore, the central part of superclusters are unique and ideal laboratories where to study this astrophysical event.

Applying a percolation algorithm to cluster catalogues, in order to individuate density enhancements of clusters over the mean density, Zucca et al. (1993) obtained catalogues of superclusters at various density excesses: among the richest structures found there are the Shapley Concentration in the Southern hemisphere and the Corona Borealis supercluster in the Northern one.

Our group already performed an extensive, multiwavelength study of the Shapley Concentration in the X-ray, optical and radio bands (Bardelli et al. 1996; Ettori et al. 1997; Bardelli et al. 1998; Venturi et al. 2000): in this region three "cluster complexes" are found, which present cluster merging events at various evolutionary stages.

In order to extend the statistics, we decided to study systems of clusters belonging to the central region of the Corona Borealis supercluster.

In this paper we present the results of Beppo-SAX observations of the cluster pairs A2061–A2067 and A2122–A2124.

The plan of the paper is the following. In Sect. 2 we introduce the Corona Borealis supercluster and in Sect. 3 and 4 we describe the data reduction and the determination of the temperature profiles and maps, respectively. In Sect. 5, 6 and 7 we present the analysis of A2061, A2067, and A2124 respectively. Finally in Sect. 8 we discuss and summarize the

⋆ e-mail: sandro.bardelli@bo.astro.it, elena.zucca@bo.astro.it

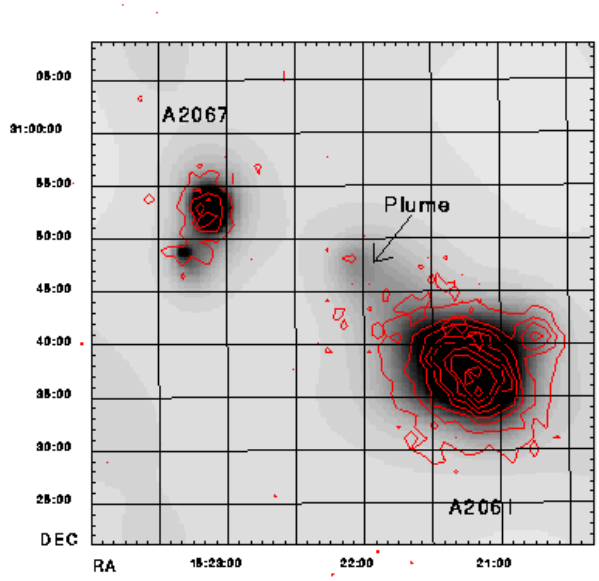

Figure 1. X-ray isodensity contours from the Beppo-SAX MECS observations of the two clusters A2061 and A2067 superimposed on the image from ROSAT PSPC. The arrow shows the gas elongation cited in the text.

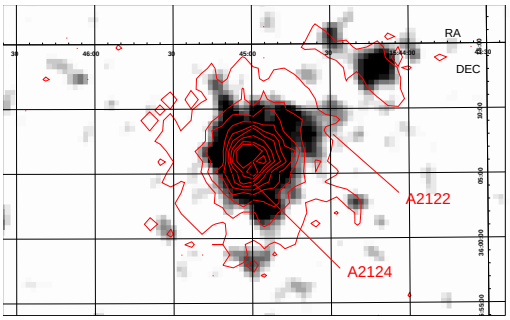

Figure 2. X-ray isodensity contours from the Beppo-SAX MECS observation of the cluster pair A2122–A2124 superimposed on the Einstein IPC image. The ACO centres of the two clusters are indicated.

results.
We assume a flat cosmology (Ω_0=1) with Ω_M=0.3, Ω_Λ=0.7 and a value for the Hubble constant of H_0=100 km s^{-1} Mpc^{-1}.

2 THE CORONA BOREALIS SUPERCLUSTER

The Corona Borealis supercluster, at $< z >\sim 0.07$ (Postman et al. 1988), is the most prominent supercluster in the Northern sky.
At an overdensity in number of clusters of $f \geqslant 2$ (Zucca et al. 1993) this supercluster is made up of ten clusters: A2019, A2056, A2061, A2065, A2067, A2079, A2089, A2092, A2122 and A2124 (see also Cappi & Maurogordato 1992).
The central part of the Corona Borealis supercluster covers a region of $6^\circ \times 6^\circ$ centred on $\alpha_{J2000} = 15^h20^m$, $\delta_{J2000} = +30^\circ$ and is made up of seven clusters: four of them (A2056, A2065, A2079 and A2089) are grouped together in the Southern part, A2061 and A2067 are close together in the Northern part, and A2092 is isolated in the North–Eastern part (see also figure 1 in Small et al. 1998).
A2122 and A2124 are located at the North-East periphery of this central region ($\sim 5^\circ$ from the centre of the supercluster).
According to Bahcall (1992) the entire supercluster extends for at least ~ 100 h^{-1} Mpc on the plane of the sky, while according to Small et al. (1997) it is only ~ 40 h^{-1} Mpc along the line of sight.
The dominant cluster of Corona Borealis is A2065 (z=0.0726, Struble & Rood 1999): located in the Southern part of the supercluster, it is the only cluster of the supercluster of richness class 2. It shows a late stage merging (Markevitch et al. 1999).
Inside this supercluster two pairs of candidate interacting clusters at high density excess have been found: A2061–A2067 ($f \geqslant 10$) and A2122–A2124 ($f \geqslant 400$). All these clusters have richness class 1.
In the present work we firstly focus on the clusters A2061 and A2067. In order to show the relative position of the two clusters, we present in Figure 1 the X-ray isophotes from the two MECS observations in the [2–10] keV energy range superimposed on a gray scale image of the existing archive ROSAT PSPC pointed observation which contains both clusters. Unfortunately, the PSPC observation is offset by ~ 42 arcmin, and therefore the PSF is degradated. It can be seen from the PSPC observation that A2061 seems to be elongated towards A2067. This plume of X-ray emission might indicate the presence of interaction between the two clusters. Note that in the Beppo-SAX data there is no trace of this elongation because part of it falls under the detector entrance window supporting structure (called strongback).
From this image we can estimate that the distance between the centres of the two clusters on the plane of the sky is ~ 30 arcmin: at the redshift of the clusters ($< z >\sim 0.076$) this distance corresponds to ~ 1.8 h^{-1} Mpc , i.e. less than 2 Abell radii (~ 3 h^{-1} Mpc). On the other hand the velocity difference between A2061 and A2067 is $\Delta v \sim 1533$ km s^{-1} (Oegerle & Hill 2001): if this Δv was due purely to Hubble flow, the separation between these two clusters would be ~ 15.44 h^{-1} Mpc , therefore too large for a cluster interaction. However this velocity difference results from the composition of the unknown relative peculiar velocity and the cosmological distance of the two clusters.
Secondly we study the clusters A2122 and A2124. These clusters are so nearby (their Δv is 150 km s^{-1}, while the distance on the plane of the sky is ~ 7 arcmin) that there are no data about them as pair in literature: there is a lot of information about A2124, while there are very few data about A2122, and sometime they are considered as a single cluster. Because of their small distance on the plane of the sky, they have been observed with a single Beppo-SAX pointing centred on the cluster A2124. In Figure 2 we present an Einstein IPC image of the diffuse gas of these clusters superimposed to the X-ray isophotes from the MECS observation in the [2–10] keV energy range: the nominal ACO centres are indicated with arrows.

Table 1. Beppo-SAX observation log (data refer to MECS).

Target	α (2000) $h\ m\ s$	δ (2000) $^o\ '\ ''$	date	exp.time ksec	count–rate cts/s	n_H 10^{20}cm^{-2}
Abell 2061	15 21 16.13	+30 36 43.93	2000 Aug 8–9	51.2	9.03×10^{-2}	1.96
Abell 2067	15 23 08.53	+30 52 51.33	2000 Jul 28–29	50.6	0.92×10^{-2}	1.98
Abell 2124	15 45 00.00	+36 03 57.60	2001 Feb 5–8	133.0	5.19×10^{-2}	1.65

3 OBSERVATIONS AND DATA REDUCTION

The clusters A2061, A2067 and A2124 were observed by the Beppo-SAX satellite (Boella et al. 1997a) in the periods 2000 August 8–9, 2000 July 28–29 and 2001 February 5–8, respectively. We discuss here the data from two of the instruments on board Beppo-SAX: the Medium–Energy Concentrator Spectrometer (MECS) and the Low–Energy Concentrator Spectrometer (LECS, used here only for A2067). The MECS (Boella et al. 1997b) is composed by two units, working in the [1–10] keV energy range. At 6 keV, the spectral resolution is $\sim 8\%$ and the angular resolution is $\sim 0.7'$ (FWHM). The LECS (Parmar et al. 1997) consists of an imaging X-ray detector, working in the [0.1–9] keV energy range, with 20% spectral resolution and $0.8'$ (FWHM) angular resolution (both computed at 1 keV). Standard reduction procedures and screening criteria have been adopted to produce linearized and equalized event files. The MECS (LECS) data preparation and linearization were performed using the SAXDAS (SAXLEDAS) package under FTOOLS environment.
We also analysed PDS (Phoswich Detector System) data for these clusters: we found that no significant detection is present for A2061 and for A2067. For A2124 we found a small excess in the [15–40] keV energy range possibly associated with the X-ray source EXSS 1543.1+3615 (Oppenheimer et al. 1997).
We have taken into account the PSF-induced spectral distortions (D'Acri et al. 1998) in the MECS analysis using effective area files produced with the *effarea* program. Note that, due to the displacements of the two MECS units, the region masked by the support window is different in MECS2 and in MECS3: this fact allows to recover, at least partly, the information in the region 8–12 arcmin from the field center. A detailed explanation of the MECS analysis is given in De Grandi & Molendi (2001). All MECS and LECS spectra have been background subtracted using spectra extracted from blank sky event files in the same region of the detector as the source (Fiore et al. 1999).
The observation log is reported in Table 1. We recall that A2122 and A2124 belong to a single Beppo-SAX observation. The coordinates reported in this table are the pointing coordinates. The observed count–rates for A2061, A2067 and A2124 for the 2 MECS units and within the central 8 arcmin (corresponding to $\sim 0.50\ \ h^{-1}$ Mpc) are also reported in the table.
Recently, Perri & Capalbi (2002) found that a systematic error affects the sky coordinates derived from the LECS and MECS instruments. The corrections depend on the spacescraft roll angle and are of the order of ~ 30 arcsec for our observations. From now on all the X-ray coordinates will be corrected for this systematic error.

4 TEMPERATURE PROFILES AND MAPS

In order to find the global temperature, we extracted a circular region of 8 arcmin (~ 0.50, ~ 0.48 and $\sim 0.40\ \ h^{-1}$ Mpc for A2061, A2067 and A2124 respectively) from the centre of the MECS data in the range [2–10] keV. This region, although smaller than the extension of the clusters, has been chosen because it is not affected by the absorption caused by the strongback. We fitted the spectrum with a *mekal* (Mewe 1995; Kaastra 1992) model with an absorbing Galactic hydrogen column (*wabs* model), as implemented in the XSPEC package (Ver. 10.00). After having checked that the fitted Galactic absorption is consistent with the literature measurement (Dickey & Lockman 1990), we fixed it to this value. The values for each cluster are reported in Table 1.
In analysing temperature profiles and maps we used only the MECS data, for which the correction for the PSF-induced spectral distortions is available. The cluster emission has been divided into concentric annuli, centred on the X-ray emission peak: out to 8 arcmin the annuli are $2'$ wide, beyond this radius the annuli are $4'$ wide.
However, we limited all the fitting procedures to the cases in which the source counts are more than 30% of the total (i.e. source plus background) counts (see the discussion in De Grandi & Molendi 2002): indeed when the source counts are low, the spectral features of the background could dominate the results.
In order to explore if there is an asymmetry of the temperature distributions we divided the cluster maps in four sectors. Sector I is North–West of the image and the numbers increase clockwise. The value of temperature referred to the 0–2 arcmin region is the same for all the sectors because a circular region was used to fit data. This analysis has been possible only for A2061 and A2124, being A2067 too faint to permit meaningful temperature determinations in sectors.

5 THE CLUSTER A2061

Abell 2061 is a cluster of richness class 1 and Bautz–Morgan class III; the ACO (Abell et al. 1989) coordinates are $\alpha_{2000} = 15^h21^m15^s$ and $\delta_{2000} = +30^h39'17''$.
On the basis of 118 redshifts Oegerle & Hill (2001) found that the biweight estimate of the observed location was C_{bi} =23699± 70 km s^{-1} and that the biweight estimate of the scale was $S_{bi}=780^{+57}_{-47}$ km s^{-1}. At the redshift of the cluster 1 arcmin corresponds to 62.70 h^{-1} kpc.
We observed this cluster using an exposure time of 51163 seconds and in Figure 3 we present the MECS isophotes in

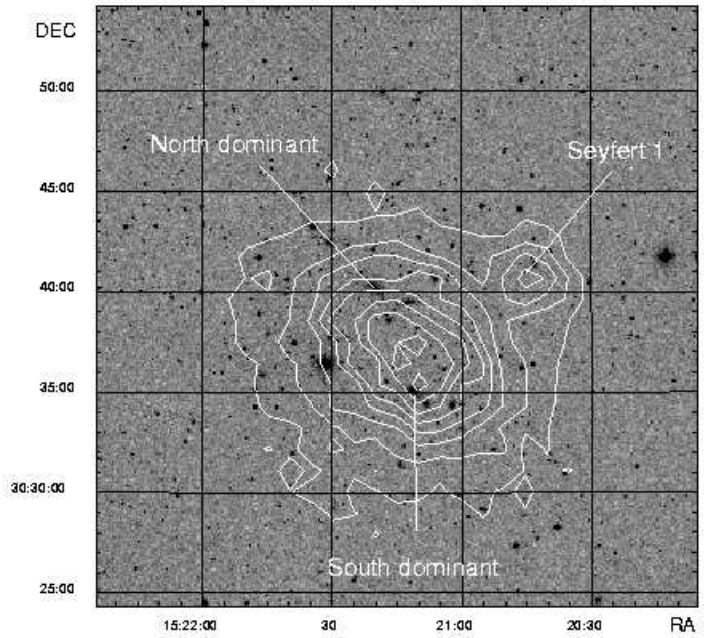

Figure 3. X-ray isophotes, from a Beppo-SAX MECS observation pointed on A2061, superimposed on the optical image from the Digital Sky Survey. The data have been smoothed with a Gaussian of 8 pixel FWHM (1 pixel=8 arcsec) and the linear step within contours is 0.34, with the lowest isophote corresponding to 0.250 cts pix^{-1}. The labelled objects are described in the text

the [2–10] keV band superimposed on the optical image from the Digital Sky Survey. The centroid of diffuse emission has coordinates $\alpha_{2000} = 15^h21^m14^s$, $\delta_{2000} = +30°37'32''$ and is 1.8 arcmin from the ACO centre, corresponding to ~ 0.11 h^{-1} Mpc . The hot gas distribution appears to be elongated in the NE–SW direction, i.e. toward A2067.

Two bright galaxies are located approximately along the major axis of the ellipse described by the isophotes. One of them (dubbed North dominant) is located 3.1 arcmin (~ 0.19 h^{-1} Mpc) NE from the X-ray centre; it has a velocity of v=23725 $\pm$ 23 km s^{-1} (Oegerle & Hill 1998) and therefore it is at rest with respect to the cluster mean velocity. The other dominant galaxy (dubbed South dominant), located 2.6 arcmin (~ 0.16 h^{-1} Mpc) SW from the X-ray centre, has a velocity of v=22720 $\pm$ 20 km s^{-1} (Oegerle & Hill 1998), and therefore it has a $\Delta v \sim 980$ km s^{-1} with respect to the centroid. The R magnitudes of the two galaxies are R_{APM}=12.24 and 12.84, respectively.

In the NW direction, at 7.9 arcmin (~ 0.50 h^{-1} Mpc) from the X-ray centre, there is a significant unresolved X-ray peak ($\alpha_{2000} = 15^h20^m45^s$, $\delta_{2000} = +30°40'58.7''$). Near this position two different objects are located: a galaxy ($\alpha_{2000} = 15^h20^m45.23^s$, $\delta_{2000} = +30°41'0.7''$; R=13.93) without a measured redshift, at $\sim$ 20.67 arcsec from the peak, and a Seyfert 1 galaxy ($\alpha_{2000} = 15^h20^m43^s$, $\delta_{2000} = +30°41'23''$; R=15.27) at $\sim$ 35 arcsec from the peak, at z=0.0772 (Small et al. 1997), that we associate to the X-ray peak.

5.1 Spatial analysis

Looking at MECS X-ray isophotes of the cluster (see Figure 3), it is clear that it is characterized by an elongated diffuse emission. For this reason we fitted the surface brightness distribution using an elliptical corrected King law

$$P(x,y) = I_o \left[1 + \left(\frac{x'}{R_1}\right)^2 + \left(\frac{y'}{R_2}\right)^2\right]^{-3\beta+0.5} + bck \quad (1)$$

where

$$x' = (x - x_k)\cos\theta + (y - y_k)\sin\theta$$
$$y' = -(x - x_k)\sin\theta + (y - y_k)\cos\theta$$

in order to take into account the inclination angle θ of the cluster. The variables to be estimated are the normalization I_o, the positions (x_k, y_k) of the centre of the cluster, the inclination angle of the cluster (θ, computed clockwise from the North), its core radii (R_1 and R_2), the exponent of the King law (β). The background (bck) has been estimated from the background map (see Sect. 3) and, after having rescaled it by the exposure times, resulted to be 0.09 cts pix^{-1}. The fit has been performed on a region of 9 arcmin radius by minimizing the χ^2 variable between the model and the data, after having masked a circle of 24$''$ diameter centered on the second X-ray peak described in Sect. 5. The resulting reduced χ^2 is 1.044 with 1254 degrees of freedom. The results of the fit, done in the [2–10] keV energy range, are reported in Table 2. We found β=0.634, while the mean value of the core radius is 0.265 h^{-1} Mpc , larger than the average value of 0.08 h^{-1} Mpc found by Ettori & Fabian (1999) from a sample of 27 clusters.

This observed large value of the core radius indicates, together with the other properties described in the previous section, that the cluster is not completely relaxed and the

Table 2. Results of the bi-dimensional fit for A2061.

Normalization	R_1	R_2	β	θ
2.199 ± 0.030 cts pix^{-1}	34.97 ± 1.50 pix	29.18 ± 1.05 pix	0.634 ± 0.023	$116^o \pm 0.8^o$
$(3.13 \pm 0.04) \times 10^{-6}$ erg str^{-1} cm^{-2} s^{-1}	0.290 ± 0.012 h^{-1} Mpc	0.242 ± 0.009 h^{-1} Mpc		

ICM is still settling after a major disturbance induced from a merger (see the discussion in Sect.8).
From the normalization of the King function it is possible to obtain the central surface brightness, using the appropriate conversion factor from counts to intrinsic flux (i.e. corrected for absorption). Assuming a bremsstrahlung emission from a hot gas with temperature of 4.52 keV, an abundance of 0.10 and a hydrogen column density of 1.96 $\times 10^{20}$ atoms cm^{-2} (see Sect. 5.2), the central surface brightness in the [2–10] keV range resulted to be I_o= 3.13 $\times 10^{-6}$ erg s^{-1} cm^{-2} str^{-1}.

5.2 Global temperature and abundance

We found that the global temperature of this cluster, obtained from the MECS instrument, is $kT = 4.52^{+0.48}_{-0.38}$ keV with an abundance of $0.10^{+0.09}_{-0.08}$, where the errors are at the 90% confidence level. The reduced χ^2 is 0.92 with 109 degrees of freedom. In Figure 4 we show the MECS spectrum of A2061, overplotted to the fit, and the corresponding confidence ellipse of the temperature and abundance parameters. We determined the temperature and the abundance also in a larger region (within 16 arcmin, corresponding to ~ 1 h^{-1} Mpc), finding $kT = 4.13^{+0.44}_{-0.38}$ keV and abundance $0.06^{+0.10}_{-0.06}$ with a reduced χ^2 of 0.98 and 127 degrees of freedom. These values are well consistent with the previous estimate.

Following the $\sigma - T$ relation of Lubin & Bahcall (1993) [$\sigma = 332\,(kT)^{0.6}$ km s^{-1}], the temperature of kT=4.52 keV implies a velocity dispersion of 821^{+30}_{-26} km s^{-1}, consistent with the value estimated by Oegerle & Hill (2001).
Another way to estimate the correspondence between the velocity dispersion and the hot gas temperature is to calculate β_{spec} (Cavaliere & FuscoFemiano 1976):

$$\beta_{spec} = \frac{\mu m_p \sigma^2}{kT}$$

where $\mu = 0.60$ is the mean molecular weight, m_p is the proton mass, σ is the velocity dispersion of galaxies and kT is the temperature of the cluster gas. Using the value obtained by Oegerle et al. for the velocity dispersion, and the temperature we found, we obtained β_{spec}=0.84, lower than the typical value of 1.1 (Sarazin 1988).
With the temperature estimated in the region 0–16 arcmin, the total luminosity within this region is $L_{[2-10]keV} = (1.21 \pm 0.02) \times 10^{44}$ h^{-2} erg s^{-1}, corresponding to a bolometric luminosity of L_X=2.45 $\times 10^{44}$ h^{-2} erg s^{-1}; the flux we obtained in the same region is $F_{[2-10]keV} = (1.72 \pm 0.03) \times 10^{-11}$ erg cm^{-2} s^{-1}. We found these two values after having subtracted the contribution of the second X-ray peak described in Sect. 5.
Ebeling et al. (1996) reported the flux for this cluster from the ROSAT All Sky Survey, assuming a temperature of 5.5 keV: they found $F_{[2-10]keV}$=1.46 $\times 10^{-11}$ erg cm^{-2} s^{-1}, i.e. 15% lower than our value. From the X-ray luminosity function of clusters in the [2–10] keV band, Edge et al. (1990) found L^*=2 $\times 10^{44}$ h^{-2} erg s^{-1}: the luminosity we estimated is 39% lower than L^*.

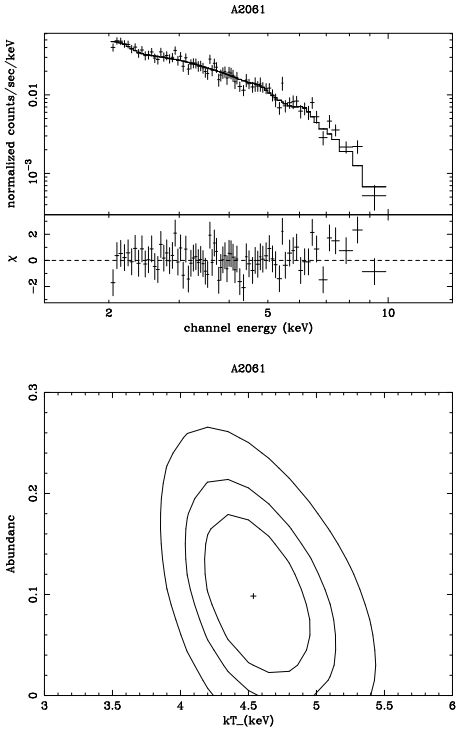

Figure 4. Spectrum and confidence ellipse of the estimated temperature and abundance on MECS data within 8 arcmin from the centre of A2061. The ellipses correspond to 68%, 90% and 99% confidence levels.

5.3 Temperature profiles and maps

The next step is the description of the temperature distribution within the cluster by dividing the frame in rings and sectors. Given the low count statistics, the abundance resulted not constrained by the data, so we fixed it to the value of 0.10, according to the value found with MECS data within 8 arcmin. The spectral analysis was performed after having masked a circle of 3′ radius centered on the second X-ray peak described in Sect. 5. This peak affects annuli 6′–8′ and 8′–12′. The results are reported in Table 3. Figure 5 shows the temperature profile of A2061 in annuli around the cluster centre. The vertical bars correspond to the 68% errors and the horizontal bars represent the bins used to extract the counts. The dotted line corresponds to the value obtained from the global temperature fit. From this figure

Table 3. Spectral results from regions of various radii (arcmin) from the centre of A2061. Errors are at 90 % and 68 % confidence level. Abundance is fixed to the value 0.10.

Radius (*arcmin*)	kT (*keV*)	Reduced χ^2 (d.o.f.)
0 - 2	$4.35^{+0.87\ +0.49}_{-0.61\ -0.38}$	0.64 (48)
2 - 4	$5.66^{+0.98\ +0.56}_{-0.74\ -0.46}$	0.79 (58)
4 - 6	$4.20^{+0.84\ +0.44}_{-0.64\ -0.38}$	1.11 (50)
6 - 8	$3.22^{+1.03\ +0.57}_{-0.67\ -0.43}$	1.02 (27)
8 - 12	$1.60^{+1.31\ +0.65}_{-0.62\ -0.41}$	0.90 (38)

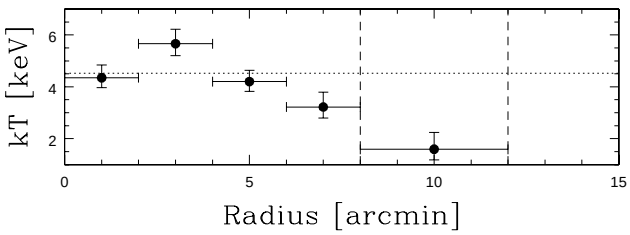

Figure 5. Temperature radial profile of A2061. The vertical bars correspond to 68% errors, while the horizontal bars represent the bins used to extract the counts. The dotted line corresponds to the global temperature, derived within 8 arcmin; vertical dashed lines indicate the region where the strongback correction is applied.

we note that the profile is slightly decreasing, a part the second point, which is higher than the global value: this is due to a temperature increase in a specific area of the cluster (see below).

In order to explore if there is an asymmetry of the temperature distribution due to the interaction of the intracluster medium with possible material of the A2067 cluster (see Figure 1), we divided the cluster map in four sectors as shown in Figure 6. Sector IV points towards the A2067 cluster. Also in this case, we masked the second X-ray peak, which is located in sector I. The results are reported in Table 4. Note that in the $8'$–$12'$ annuli, sectors I, II and III, the source counts are 20.0 %, 17.8% and 18.7%, respectively, of the

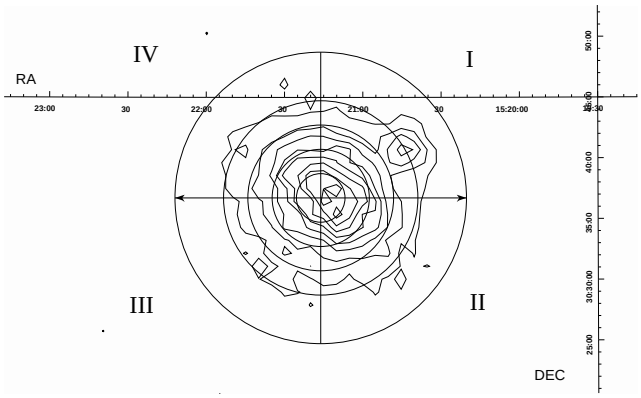

Figure 6. Beppo-SAX MECS image of A2061. The concentric circles correspond to the bins of the radial profiles, while the quadrants correspond to the sectors used for the temperature map analysis.

Table 4. Spectral results from regions of various radii (arcmin) from the centre of A2061. Errors are at 90 % and 68 % confidence level. Abundance is fixed to the value 0.10. Sectors indicated in italic are those where the source counts are lower than 30% of the total.

R (*arcmin*)	Sector	kT (*keV*)	Reduced χ^2 (d.o.f.)
2 - 4	I	$4.27^{+1.45\ +0.80}_{-0.95\ -0.62}$	0.65 (46)
	II	$4.65^{+1.45\ +0.81}_{-0.95\ -0.61}$	0.45 (49)
	III	$4.78^{+2.19\ +1.14}_{-1.20\ -0.78}$	0.41 (37)
	IV	$10.67^{+8.35\ +3.90}_{-3.60\ -2.47}$	0.66 (44)
4 - 6	I	$2.91^{+1.29\ +0.72}_{-0.71\ -0.45}$	0.57 (46)
	II	$5.23^{+2.65\ +1.39}_{-1.46\ -0.98}$	0.64 (34)
	III	$5.05^{+5.33\ +2.40}_{-2.00\ -1.40}$	0.69 (49)
	IV	$3.96^{+1.40\ +0.73}_{-0.90\ -0.60}$	0.58 (24)
6 - 8	I	$4.53^{+20.60\ +9.25}_{-2.64\ -1.83}$	0.36 (57)
	II	$3.80^{+3.76\ +1.75}_{-1.51\ -1.07}$	0.40 (39)
	III	$2.50^{+1.69\ +0.86}_{-0.84\ -0.55}$	0.79 (06)
	IV	$2.39^{+2.29\ +1.08}_{-1.10\ -0.76}$	0.31 (36)
8 - 12	*I*	$2.55^{+20.50\ +3.45}_{-1.65\ -1.05}$	*0.41* (*11*)
	II	$2.13^{+1.60\ +0.80}_{-0.81\ -0.55}$	*1.10* (*13*)
	III	$1.08^{+1.27\ +0.64}_{-0.49\ -0.33}$	*1.53* (*12*)
	IV	$2.77^{+1.19\ +0.63}_{-0.75\ -0.49}$	1.10 (18)

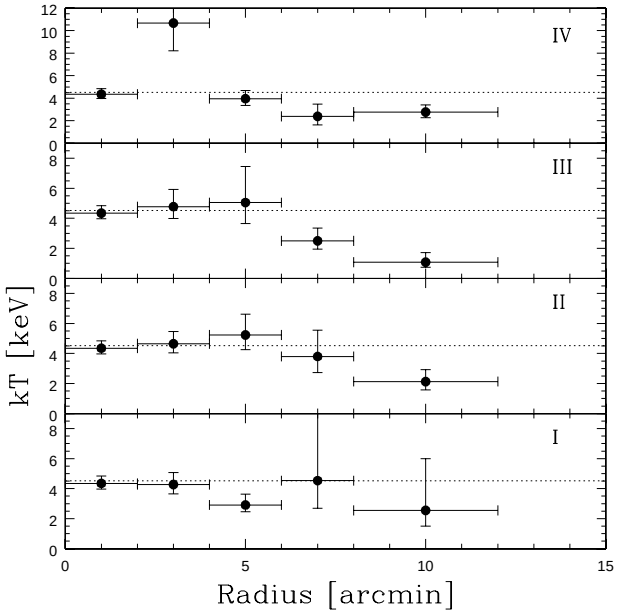

Figure 7. Temperature map of A2061. The vertical bars correspond to 68% errors, while the horizontal bars represent the bins used to extract the counts. Dotted lines correspond to the global temperature fit. For the first bin a circular region was used to fit data, consequently the value is the same for all quadrants.

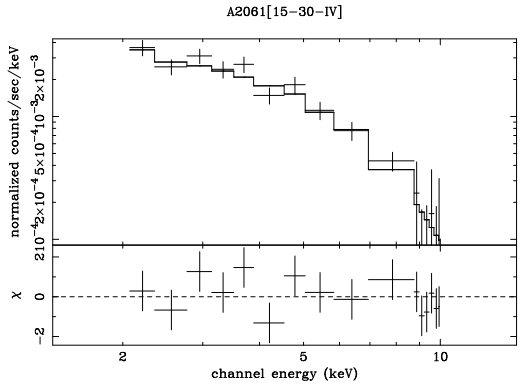

Figure 8. Spectrum, fit and residuals of the MECS data in the $2'$–$4'$ arcmin annulus, sector IV, for A2061.

total counts, that is the background contribution becomes dominant. In Figure 7 the temperature profiles in the four sectors are presented. Looking at the image it is possible to note that the temperature distribution is quite isothermal up to 8 arcmin, with the exception of sector IV, for which there is a remarkable increase of the temperature around the 3 arcmin bin which is not consistent (at 2.5 sigma) with that of the global fit. This result leads us to suppose that the discrepancy with respect to the global value found in the temperature radial profile in the $2'$–$4'$ arcmin annulus (see Figure 5) is due to the presence of this excess.

The spectral fit of the data in the 2–4 region of sector IV is shown in Figure 8: the temperature is $kT = 10.67^{+3.90}_{-2.47}$ keV (the errors are at the 68% confidence level) and the reduced χ^2 is 0.96 with 44 degrees of freedom.

In order to check the robustness of the temperature determined in this region, we repeated the fit, forcing the abundance to different values in the range 0.00–1.00: the derived temperatures are in the range 9.06–11.45 keV, in any case not consistent with the value from the global fit. Moreover we checked whether the data could be described by a bremsstrahlung plus a power law: the fit, although formally acceptable, does not constraint the photon index of the power law.

This result might suggest the presence of a candidate internal shock due to the merger of an infalling group into the main body of the cluster, as we discuss in Sect. 8.

6 THE CLUSTER A2067

Abell 2067 is a cluster of richness class 1 and Bautz-Morgan class III; its centre has coordinates $\alpha_{2000} = 15^h23^m14^s$, $\delta_{2000} = +30°54'23''$ (Abell et al. 1989). On the basis of 44 redshifts, Oegerle & Hill (2001) estimated C_{bi}=22166± 79 km s^{-1} and S_{bi}=536^{+69}_{-90} km s^{-1}. At the redshift of the cluster 1 arcmin corresponds to 59.98 h^{-1} kpc.

In Figure 9 we present the MECS X-ray isophotes superimposed on the optical image from the Digital Sky Survey: the isodensity contours of the cluster are taken in the energy range [2–10] keV. The centroid of diffuse emission has coordinates $\alpha_{2000} = 15^h23^m08^s$, $\delta_{2000} = +30°53'05''$ and is 1.9 arcmin from the ACO centre, corresponding to $\sim$ 0.11 h^{-1} Mpc . This cluster does not appear significantly elongated but shows a diffuse excess in the Southern part, in correspondence of a galaxy overdensity. Kopylova & Kopylov (1998) reported that A2067 is characterized by the presence of a central dominant galaxy ($\alpha_{2000} = 15^h24^m00^s$, $\delta_{2000} = +31°12'40''$), but we found that this object is 22.6 arcmin (1.36 h^{-1} Mpc) far from the X-ray centre. Studying the morphological classification of galaxies which belong to A2067 we found out two dominant galaxies: one of them, a central dominant galaxy, is located 0.5 arcmin ($\sim$ 0.03 h^{-1} Mpc) from the X-ray centre, has a velocity of v=22061 ± 54 km s^{-1} (Postman et al. 1988) and its R_{APM} magnitude is 12.44. The other dominant galaxy, with a velocity of v=21576 ± 50 km s^{-1} (Postman et al. 1988) is located 4.3 arcmin ($\sim$ 0.26 h^{-1} Mpc) from the X-ray centre ($\alpha_{2000} = 15^h23^m08^s$, $\delta_{2000} = +30°48'46''$) and its R_{APM} magnitude is 15.97. These dominant galaxies are indicated as cD and D in Figure 9.

6.1 Global temperature and abundance

Fitting the data extracted from a circular region of 8 arcmin from the centre of the MECS data in the range [2–10] keV we found $kT = 1.73^{+0.38}_{-0.37}$ keV (errors are at the 90% confidence level) with a reduced χ^2 of 1.52 with 46 degrees of freedom, but the abundance is not constrained. Therefore in order to use all the information present in the Beppo-SAX observation, we considered also the data of the LECS instrument in the [0.2–3] keV band extracted from the same region: we obtained $kT = 1.44^{+0.38}_{-0.30}$ keV and an abundance of $0.18^{+0.42}_{-0.16}$, with a reduced χ^2 of 1.08 with 16 degrees of freedom. The temperature is consistent with the MECS value.

We have repeated the fit with the MECS data in the region 0–8 arcmin fixing the abundance to the value found from LECS data: we obtained $kT = 1.67^{+0.37}_{-0.31}$ keV with a reduced χ^2 of 1.50 with 47 degrees of freedom.

Finally we used the combined LECS+MECS data. In this case, we ran the fits by estimating also the relative normalization between the two instruments: we obtained a value similar to that found by Bardelli et al. (2002) and by Ettori et al. (2000). Therefore we fixed it to the value 0.50. From the LECS+MECS data we found $kT = 1.54^{+0.26}_{-0.22}$ keV and an abundance of $0.19^{+0.30}_{-0.16}$, with a reduced χ^2 of 1.39 with 64 degrees of freedom. The temperature is consistent at 0.6 sigma with that obtained from MECS data and at 0.4 sigma with that obtained from LECS data; the abundance is consistent at 0.1 sigma with the value found out from LECS data. In Figure 10 we show the combined LECS+MECS spectrum of A2067, overplotted to the fit.

The temperature of kT=1.54 keV implies a velocity dispersion of 430^{+26}_{-24} km s^{-1} (errors are at 68% confidence level) which is consistent with the value estimated by Oegerle & Hill (2001).

From MECS data we found that the total luminosity within 8 arcmin is $L_{[2-10]keV} = (0.58 \pm 0.04) \times 10^{43}$ h^{-2} erg s^{-1}, corresponding to a bolometric luminosity of L_X=2.11 $\times 10^{43}$ h^{-2} erg s^{-1}. According to McKee et al. (1980), the X-ray luminosity in the range [2–10] keV of A2067 is $L_{[2-10]keV} <$ 1.31 $\times 10^{43}$ h^{-2} erg s^{-1}. Our value is $\sim$ 97% lower than the L^* value given by Edge et al. (1990).

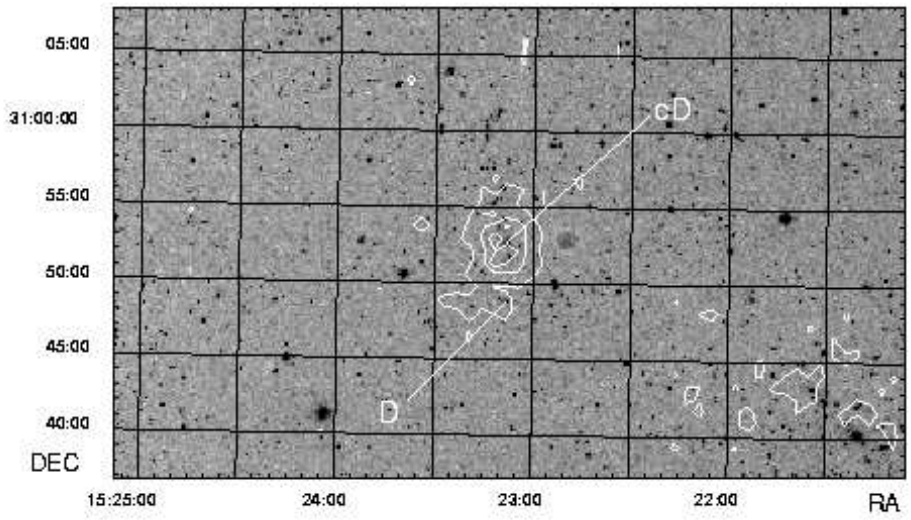

Figure 9. X-ray isophotes, from a Beppo-SAX MECS observation pointed on A2067, superimposed on the optical image from the Digital Sky Survey. The data have been smoothed with a Gaussian of 6 pixel FWHM (1 pixel=8 arcsec) and the linear step within contours is 0.22, with the lowest isophote corresponding to 0.250 cts pix^{-1}. The labelled objects are described in the text.

Table 5. Spectral results from regions of various radii (arcmin) from the centre of A2067. Errors are at 90 % and 68 % confidence level. Abundance is fixed to the value 0.18. Regions indicated in italic are those where the source counts are lower than 30% of the total.

Radius (*arcmin*)	kT (*keV*)	Reduced χ^2 (d.o.f.)
0 - 2	$1.96^{+0.41\ +0.24}_{-0.32\ -0.20}$	1.91 (13)
2 - 4	$1.28^{+0.49\ +0.28}_{-0.34\ -0.22}$	1.22 (11)
4 - 6	$1.76^{+1.41\ +0.68}_{-0.74\ -0.50}$	*1.16 (15)*

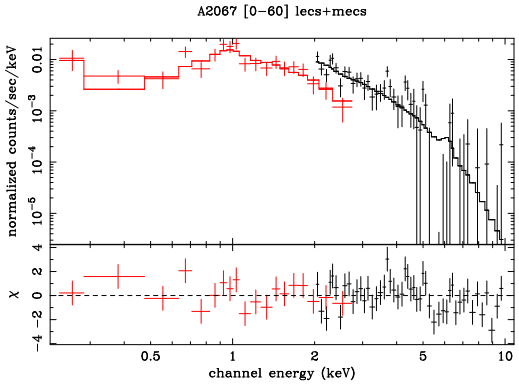

Figure 10. Spectrum of LECS+MECS data within 8 arcmin from the centre of A2067.

6.2 Temperature profiles

In analysing temperature profiles we fixed the abundance to the value of 0.18, according to the value found with LECS data. The results are reported in Table 5. Note that in the 4′–6′ annulus the source counts are 27.1 % of the total counts, i.e. lower than 30% of the total and therefore on the border of our acceptability criterium. In Figure 11 we report the temperature profile of A2067 in annuli around the cluster centre. Looking at the figure it is possible to note that the temperature is roughly constant, i.e. it is isothermal up to 6 arcmin ($\sim 0.36\ \ h^{-1}$ Mpc).
Given the low statistics of counts we were not able to divide the cluster in sectors as done for A2061 and it was not possible to do a bidimensional analysis.

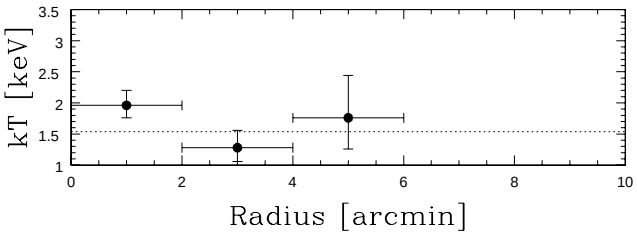

Figure 11. Temperature radial profile of A2067. The vertical bars correspond to 68% errors, while the horizontal bars represent the bins used to extract the counts. The dotted line corresponds to the global temperature fit, derived within 8 arcmin.

7 THE CLUSTER A2124

Abell 2124 is a richness class 1 cluster and Bautz-Morgan class I; its centre has coordinates $\alpha_{2000} = 15^h44^m59^s$, $\delta_{2000} = +36°04'$ (Abell et al. 1989). On the basis of 61 redshifts Oegerle & Hill (2001) estimated C_{bi}=19684± 110 km s^{-1} and S_{bi}=862^{+91}_{-69} km s^{-1}. At the redshift of the cluster 1 arcmin corresponds to 52.92 h^{-1} kpc.
We observed this cluster with an exposure time of 133017

seconds. In Figure 12 we present the MECS X-ray isophotes superimposed on the optical image from the Digital Sky Survey. The X-ray centre has coordinates $\alpha_{2000} = 15^h44^m56^s$, $\delta_{2000} = +36°06'04''$. A2124 is dominated by a single cD galaxy ($\alpha_{2000} = 15^h44^m59^s$, $\delta_{2000} = +36°06'34''$), with a velocity of v=19810 km s^{-1} and R magnitude of 12.49 (Kopylova & Kopylov 1998). Blakeslee & Metzger (1999) identified an arclike object at z=0.573 located 27 arcsec along the major axis from the centre of this cD galaxy.
As discussed in Sect. 2., in this Beppo-SAX observation another Abell cluster (A2122) is included with a position NW from A2124 (in Figure 12 we indicate the ACO centre of both clusters). Abell 2122 is reported as a cluster of richness 1 and Bautz-Morgan class II-III; its centre has coordinates $\alpha_{2000} = 15^h44^m29^s$, $\delta_{2000} = +36°08'$ (Abell et al. 1989) and its velocity is v=19830 km s^{-1} (Struble & Rood 1999). There is apparently a lot of confusion in the literature about A2122 and A2124. These two clusters are at a projected separation of 7.3 arcmin. Abell (1958) classified both of them as richness 1 clusters, but assigned distance class 3 to A2122 and distance class 5 to A2124. Looking at the DSS images centred on the two clusters, A2124 appears indeed as a poorer concentration of fainter galaxies 3 arcmin South to the cD (but at the same right ascension). However, the centre of A2122 falls West of the cD, in a region which apparently does not correspond to any significant galaxy concentration. Quite confusingly, in the NED database only A2122 is associated to a Zwicky cluster, while the SIMBAD database gives wrong coordinates for A2122, $\alpha_{2000} = 15^h44^m48^s$ and $\delta_{2000} = 36^o06'00''$ (instead of $\alpha_{2000} = 15^h44^m29^s$ and $\delta_{2000} = 36^o07'38''$, as reported in NED). The available redshift measurements show that the two clusters are at the same distance, at $z \sim 0.066$: this means that the separation of 7.3 arcmin corresponds to only ~ 0.39 h^{-1} Mpc; on this basis and taking into account the X–ray map, we conclude that A2122 and A2124 should be identified with the same cluster.

7.1 Spatial analysis

As done in Sect. 5.1., we fitted the surface brightness distribution using an elliptical King law; the background (*bck*) has been estimated from the background map, and resulted to be 0.205 cts pix^{-1}. The resulting reduced χ^2 is 0.956 with 1254 degrees of freedom. The results of the fit, done in the [2–10] keV energy range and within a region of 9 arcmin radius, are reported in Table 6. We found β=0.586, while the average value of the core radius is 0.122 h^{-1} Mpc .
With these values and the temperature profile (see Sect.7.3) we derive a total mass within 0.45 h^{-1} Mpc of 1.11×10^{14} h^{-1} M$_\odot$.

7.2 Global temperature and abundance

For the MECS global temperature we found kT=$4.41^{+0.38}_{-0.33}$ keV and an abundance of $0.29^{+0.10}_{-0.09}$, where the errors are at the 90% confidence level. The reduced χ^2 is 0.98 with 132 degrees of freedom.
The temperature found implies a velocity dispersion of 809^{+24}_{-23} km s^{-1} (errors are at 68% confidence level), which is consistent with the value estimated by Oegerle & Hill (2001).
Using the value obtained by Oegerle for the velocity dispersion, and the temperature we found from MECS data in the 0-8 arcmin region, we obtained β_{spec}=1.05, similar to the typical value of 1.1 (Sarazin 1988).
From MECS data we found that the total luminosity within 8 arcmin is $L_{[2-10]keV} = (2.82 \pm 0.04) \times 10^{43}$ h^{-2} erg s^{-1}, corresponding to a bolometric luminosity of L_X=0.56 $\times 10^{44}$ h^{-2} erg s^{-1}; the flux we obtained in the same region is $F_{[2-10]keV} = (0.58 \pm 0.01) \times 10^{-11}$ erg cm^{-2} s^{-1} to be compared with $F_{[2-10]keV}$=0.48 $\times 10^{-11}$ erg cm^{-2} s^{-1}, estimated by Ebeling et al. (1996). The luminosity we estimated is 86% lower than the L^* value given by Edge et al. (1990).

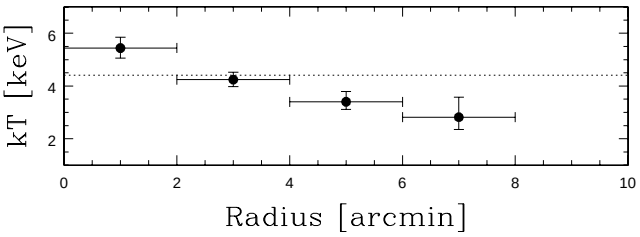

Figure 13. Temperature radial profile of A2124. The vertical bars correspond to 68% errors, while the horizontal bars represent the bins used to extract the counts. The dotted line corresponds to the global temperature fit, derived within 8 arcmin.

7.3 Temperature profiles and maps

In analysing temperature profiles we used the MECS data, and divided the cluster emission in the same way as done for A2061 and A2067 (see Sect. 5.3 and 6.2). Abundance is fixed to the value of 0.29, according to the value found from the global fit. The results are reported in Table 7. In Figure 13 we report the temperature profile of A2124 in annuli around the cluster centre. Looking at the figure it can be seen that the temperature is not constant, but shows a decrease with the radius increase.
In order to explore if there is an asymmetry of the temperature distribution, we divided the cluster map in four sectors as shown in Figure 14. The cluster A2122 belongs to the sector I, annulus 6–8 arcmin, and, unfortunately, part of its emission falls under the strongback. The results of the analysis are reported in Table 8. Note that in the 8′–12′ annulus, sector I, the source counts are 28.9 % of the total counts, while in the remaining sectors of the same annulus the source counts are lower than 16%, that is the background contribution becomes dominant. In Figure 15 the temperature profiles in the four sectors are presented. For the 0–2 arcmin region a circular region was used to fit data.
Because of a shift between the X-ray centroid and the MECS centre, the strongback support falls partly in the 6′–8′ annulus: this fact causes a loss of counts in sectors I and IV, which produces bad constraints in the temperature determination, seen as exceedingly high 90% errors (see Table 8).

Table 6. Results of the bi-dimensional fit for A2124.

Normalization	R_1	R_2	β	θ
5.189 ± 0.050 cts pix^{-1}	18.38 ± 0.50 pix	16.13 ± 0.65 pix	0.586 ± 0.010	$95^o \pm 2^o$
$(2.91 \pm 0.03) \times 10^{-6}$ erg str^{-1} cm^{-2} s^{-1}	0.130 ± 0.004 h^{-1} Mpc	0.114 ± 0.005 h^{-1} Mpc		

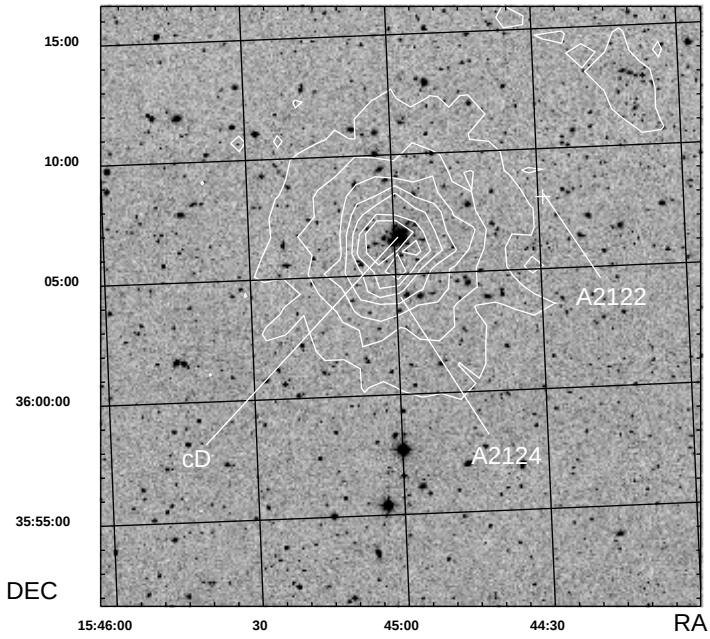

Figure 12. X-ray isophotes, from a Beppo-SAX MECS observation, of the cluster A2124, superimposed on the optical image from the Digital Sky Survey. The data have been smoothed with a Gaussian of 6 pixel FWHM (1 pixel=8 arcsec) and the linear step within contours is 0.50, with the lowest isophote corresponding to 0.571 cts pix^{-1}. The labelled objects are described in the text.

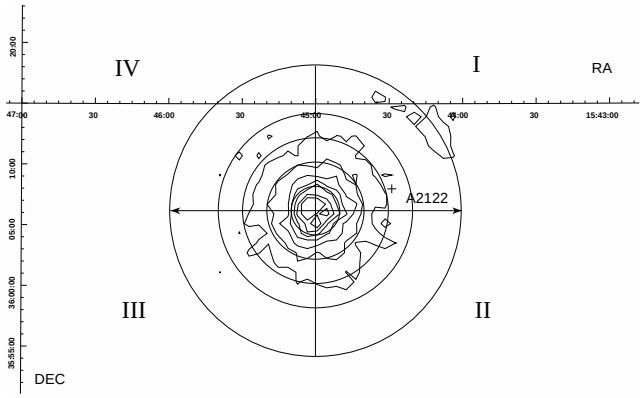

Figure 14. Beppo-SAX MECS image of A2124. The concentric circles correspond to the bins of the radial profiles, while the quadrants correspond to the sectors used for the temperature map analysis. The small cross indicates the ACO centre of A2122.

Table 7. Spectral results from regions of various radii (arcmin) from the centre of A2124. Errors are at 90 % and 68 % confidence level. Abundance is fixed to the value 0.29.

Radius (*arcmin*)	kT (*keV*)	Reduced χ^2 (d.o.f.)
0 - 2	$5.44^{+0.71\ +0.41}_{-0.61\ -0.38}$	0.81 (73)
2 - 4	$4.24^{+0.48\ +0.28}_{-0.41\ -0.26}$	1.07 (81)
4 - 6	$3.40^{+0.58\ +0.39}_{-0.46\ -0.29}$	0.91 (66)
6 - 8	$2.82^{+1.40\ +0.76}_{-0.75\ -0.47}$	1.10 (40)

8 DISCUSSION AND CONCLUSIONS

The aim of this work has been to study the gas temperature distribution of two pairs of clusters (A2061–A2067 and A2122–A2124) located in the inner part of the Corona Borealis supercluster, using Beppo-SAX observations.

Although the emission of A2122 falls under the window support of the detector, in the region between the centres of A2122 and A2124 we did not find any evidence of interaction. Also for the pair A2061–A2067 we did not find any clear sign of interaction: on one side A2061 is significantly elongated towards A2067, but on the other hand the velocity difference Δv between the two clusters is too large to be entirely due to peculiar velocity. In order to have an estimate of the relative peculiar motion we assumed a simple model for the collapse of two bodies approaching from infinity. We derived the masses of A2061 and A2067 using the $M - kT$ relation Yee & Ellingson (2003), finding $v_{pec} \simeq$

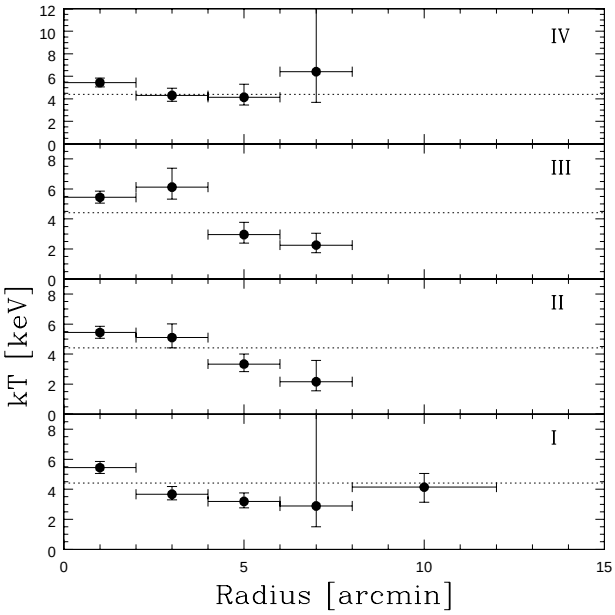

Figure 15. Temperature map of A2124. The vertical bars correspond to 68% errors, while the horizontal bars represent the bins used to extract the counts. Dotted lines correspond to the global temperature fit. For the first bin a circular region was used to fit data.

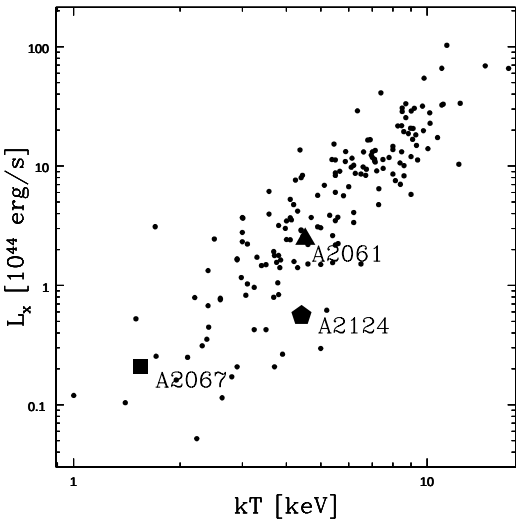

Figure 16. L_X–T relation as determined from Wue et al. (1999) for a subsample of 167 clusters. The triangle represents the location of the cluster A2061, the square corresponds to A2067 and the pentagon is for A2124.

390 km s^{-1}, i.e. only 25% of the Δv, therefore the distance between A2061 and A2067 is too large to have significant effects on the intracluster medium.
In Table 9 we summarize some information about these clusters obtained during our study.
In Figure 16 we show the $L_X - T$ relation for a sample of 167 clusters from Wue et al. (1999), adding our data for A2061 (triangle), A2067 (square) and A2124 (pentagon).

Table 8. Spectral results from regions of various radii (arcmin) from the centre of A2124. Errors are at 90 % and 68 % confidence level. Abundance is fixed to the value 0.29. Sectors indicated in italic are those where the source counts are lower than 30% of the total.

R (*arcmin*)	Sector	kT (*keV*)	Reduced χ^2 (d.o.f.)
2 - 4	I	$3.67^{+0.85\ +0.51}_{-0.58\ -0.37}$	1.77 (27)
	II	$5.10^{+1.67\ +0.91}_{-1.06\ -0.69}$	0.52 (26)
	III	$6.12^{+2.31\ +1.26}_{-1.29\ -0.79}$	1.59 (28)
	IV	$4.30^{+1.16\ +0.65}_{-0.80\ -0.52}$	1.06 (32)
4 - 6	I	$3.19^{+0.99\ +0.56}_{-0.66\ -0.43}$	1.02 (20)
	II	$3.34^{+1.21\ +0.66}_{-0.76\ -0.50}$	1.33 (20)
	III	$2.96^{+1.45\ +0.82}_{-0.81\ -0.56}$	0.74 (18)
	IV	$4.14^{+2.27\ +1.17}_{-1.16\ -0.78}$	0.56 (17)
6 - 8	I	$2.89^{+97.11\ +6.78}_{-99.07\ -1.39}$	0.15 (82)
	II	$2.16^{+3.46\ +1.42}_{-0.91\ -0.61}$	1.52 (12)
	III	$2.26^{+1.56\ +0.79}_{-0.76\ -0.50}$	0.94 (15)
	IV	$6.41^{+56.64\ +9.52}_{-3.60\ -2.72}$	0.26 (12)
8 - 12	*I*	$\mathit{4.14}^{+2.20\ +0.92}_{-1.47\ -1.01}$	*1.29* (*37*)

Looking at this figure it can be seen that all the studied clusters are in agreement with the relation. It can also be noticed that A2067 is more similar to a galaxy group than to a cluster, given its low temperature and its position in the $L_X - T$ plane.
Analysing temperature profiles and maps of these clusters we found that their temperature distributions do not show strong deviations from an isothermal behaviour. The only exception is represented by a region in A2061: we found that, in the bin 2–4 arcmin sector I, there is a significant increase of temperature (kT=$10.67^{+3.90}_{-2.47}$ keV) which is not consistent at 2.5 sigma with that of the global fit (kT=$4.52^{+0.28}_{-0.24}$ keV). This feature likely corresponds to the presence of an internal shock.
Our scenario is that a group is falling inside A2061 and forms the shock in the major cluster. The infall is along the axis individuated by the elongation of the cluster ($\sim 116^{\circ}$), as shown in Figure 17, that summarizes the geometry projected on the plane of the sky. Note that in the same direction, but on the opposite side, at ~ 18 arcmin (~ 1.05 h^{-1} Mpc) from the X-ray centre, a relic is located, a radio source normally associated with an ongoing merging (Kempner & Sarazin 2001). However, the spatial resolution of Beppo-SAX is not able to separate the emission of the infalling group from that of A2061.
This hypothesis is consistent with the behaviour of the two dominant galaxies: the North D galaxy is at rest in the velocity space with respect to the cluster, but is significantly offset with respect to the centre of the X-ray emission (at a projected distance of ~ 0.19 h^{-1} Mpc). At a projected distance of ~ 0.16 h^{-1} Mpc from the X-ray centre there is another dominant galaxy, which has a velocity difference with respect to the cluster of $\Delta v \sim 980$ km s^{-1}. It is important to note that both the dominant galaxies axis inclina-

tions ($\sim 149^\circ$ and $\sim 132^\circ$, respectively) are similar to that of the merger axis.
By studying the bidimensional distribution of optical galaxies we found a significant galaxy excess in the position reported as a square in Figure 17. It is likely that these galaxies are part of the infalling group.
We suppose that the group and A2061 are in the phase of interaction in which the cores have not encountered yet: in this phase the formation of a shock between the cores is expected. If the gas within the shocked region is nearly isothermal, we can calculate the ratio between the velocities after (u_0) and before (u_1) the shock (Markevitch et al. 1999, equation (2)) as:

$$\kappa \equiv \frac{u_1}{u_0} \cong 0.41 \pm 0.03 \ ,$$

where we used the temperatures $T_0 = 4.65$ keV and $T_1 = 10.67$ keV. We used for T_0 the value derived for sector II, annulus 2–4 arcmin, which is specular to the shock position with respect to the cluster center.
Given this value, the expected surface brightness ratio is:

$$\frac{S_{X1}}{S_{X0}} \sim 6 \ .$$

Actually we find that the ratio between the counts in the bin 2–4 arcmin sector IV (position of the shock) and II (at a specular position with respect to the centre of the cluster) is nearly 1. This inconsistency is probably due to the fact that the region interested by the interaction is much smaller than the analysed bin and than the MECS PSF. From simulations, produced with the same characteristics of our observations, we estimated that this shock could be detected only if its sizes exceed $\sim 30 \times 70 \ \ \mathrm{h}^{-1}$ kpc .
A higher spatial resolution of observation (f.i. with Chandra or XMM) is needed to assess this scenario.
The resulting difference of the gas flow after and before the shock is (Markevitch et al. 1999, equation (1)):

$$v_{col} = 2 \cdot (u_0 - u_1) \cong 2896^{+804}_{-588} \ \mathrm{km\,s^{-1}}$$

where we assume a plasma with mean molecular weight $\mu = 0.60$. Note that this value of v_{col} is similar to that of the cluster A3667 (Markevitch et al. 1999).
On the other hand, if we assume that the kinetic energy is completely converted into thermal energy, following Shibata et al. (1999), we find:

$$v_{col} = \left[\frac{3k(T_1 - T_0)}{\mu m_p}\right]^{1/2} \cong 1735^{+399}_{-293} \ \mathrm{km\,s^{-1}} \ .$$

These two values found for v_{col}, arising from different physical hypotheses, can be considered as upper and lower limits. This velocity range corresponds to a Mach number in the range

$$2.4 < M < 3.9 \ .$$

These values can be compared with the typical value of $M \sim 1.4$ given by the semi-analytical models by Gabici & Blasi (2003): however, considering the Mach number distribution of mergers happened in the last one billion years, the same authors (see their figure 8) show a significant tail at $M \sim 3$.
In conclusion, the global scenario can be the following.
A group of galaxies, arriving from North–East, impacted on the cluster A2061. As a consequence of the interaction of these two structures, the galaxies of the group precede its intracluster medium, as predicted by numerical simulation (see e.g. Tormen et al. 2003). Indeed the X-ray emission excess seen in Figure 1 North–East of A2061 (labelled as Plume) could be the remnant of the group ICM, while its galaxies can be located in correspondence of the optical overdensity shown in Figure 17.
The fact that the merging axis points towards A2067 can be an indication of the existence of a filament, on which both A2061 and A2067 lie and along which the group merged in A2061.

ACKNOWLEDGMENTS

This research has made use of linearized event files produced at the Beppo-SAX Science Data center. This work has been partially supported by the Italian Space Agency grants ASI-I-R-037-01 and ASI-I-R-063-02, and by the Italian Ministery (MIUR) grant COFIN2001 "Clusters and groups of galaxies: the interplay between dark and baryonic matter". This research has made use of the NASA/IPAC Extragalactic Database (NED) which is operated by the Jet Propulsion Laboratory, California Institute of Technology, under contract with the National Aeronautics and Space Administration. This research has made use of the SIMBAD database, operated at CDS, Strasbourg, France. We thank the referee (dr. H.Ebeling) for helpful comments.

REFERENCES

Abell G.O., 1958, ApJS, 3, 211
Abell G.O., Corwin H.G.Jr., Olowin R.P., 1989, ApJS, 70, 1
Bahcall J.N., 1992, in Clusters and Superclusters of Galaxies, ed. A. Fabian (Dordrecht: Kluwer), 275
Bardelli S., Zucca E., Malizia A., Zamorani G., Scaramella R., Vettolani G., 1996, A&A, 305, 435
Bardelli S., Zucca E., Zamorani G., Vettolani G., Scaramella R., 1998, MNRAS, 296, 599
Bardelli S., Venturi T., Zucca E., De Grandi S., Ettori E., Molendi S., 2002, A&A, 396, 65
Blakeslee J.P., Metzger M.R., 1999, ApJ, 513, 592
Boella G., Butler R.C., Perola G.C., Piro L., Scarsi L., Bleeker J.A.M., 1997a, A&AS, 122, 299
Boella G., et al., 1997b, A&AS, 122, 327
Cappi A., Maurogordato S., 1992, A&A, 259, 423
Cavaliere A., Fusco-Femiano R., 1976, A&A, 49, 137
D'Acri F., De Grandi S., Molendi S., 1998, Nucl.Phys., 69/1-3, 581
De Grandi S., Molendi S., 2001, ApJ, 551, 153
De Grandi S., Molendi S., 2002, ApJ, 567, 163
Dickey J.M., Lockman F.J., 1990, ARA&A, 28, 215
Ebeling H., Voges W., Böhringer H., Edge A.C., Huchra J.P., Briel U.G., 1996, MNRAS, 281, 799
Edge A.C., Stewart G.C., Fabian A.C., Arnaud K.A., 1990, MNRAS, 245, 599
Ettori S., Fabian A.C., White D.A., 1997, MNRAS, 289, 787
Ettori S., Fabian A.C., 1999, MNRAS, 305, 843

Table 9. General information about A2061, A2067 and A2124. C_{bi} and S_{bi} are taken from Oegerle & Hill (2001), while the other quantities are derived from our analysis (see the text). Errors on temperatures are at the 90% confidence level.

Cluster	kT_{global} keV	L_{bol} erg s^{-1}	$F_{[2-10]keV}$ erg cm^{-2} s^{-1}	$L_{[2-10]keV}$ erg s^{-1}	C_{bi} km s^{-1}	S_{bi} km s^{-1}
Abell 2061	$4.52^{+0.48}_{-0.38}$	2.45×10^{44} h^{-2}	1.72×10^{-11}	$1.21 \times 10^{44} h^{-2}$	23699 ± 70	780^{+57}_{-47}
Abell 2067	$1.54^{+0.26}_{-0.22}$	0.21×10^{44} h^{-2}	8.62×10^{-13}	$0.58 \times 10^{43} h^{-2}$	22166 ± 79	536^{+69}_{-90}
Abell 2124	$4.41^{+0.38}_{-0.33}$	0.56×10^{44} h^{-2}	0.58×10^{-11}	$0.28 \times 10^{44} h^{-2}$	19684 ± 110	862^{+91}_{-69}

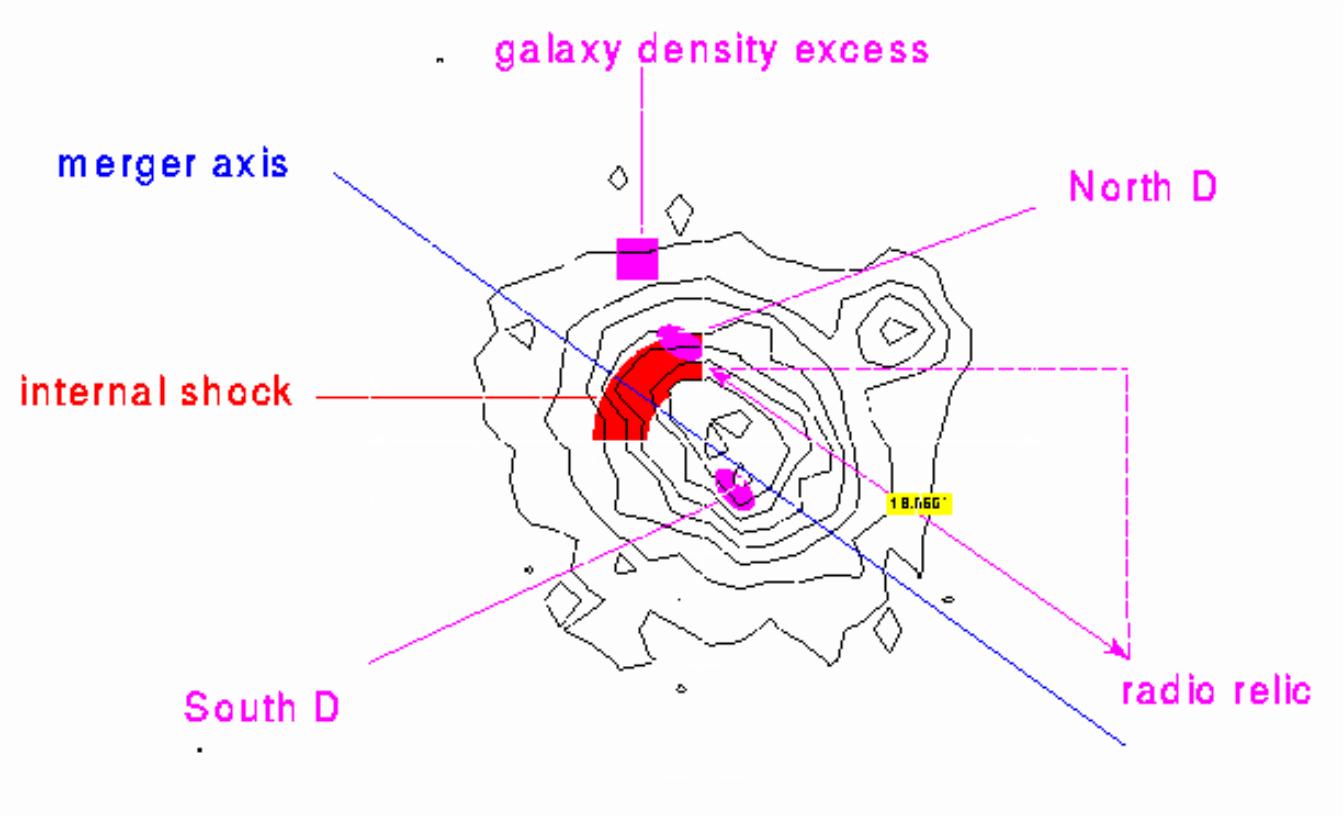

Figure 17. Plan of the cluster A2061. See the text for the labelled objects

Ettori S., Bardelli S., De Grandi S., Molendi S., Zamorani G., Zucca E., 2000, MNRAS, 318, 239

Fiore F., Guainazzi M., Grandi P., 1999, Cookbook for Beppo-SAX NFI Spectral Analysis

Gabici S., Blasi P., 2003, ApJ, 583, 695

Kaastra J.S., 1992, An X-Ray Spectral Code for Optically Thin Plasma, Internal SRON-Leiden report, updated version 2.0

Kempner J.C., Sarazin C.L., 2001, ApJ, 548, 639

Kopylova F.G., Kopylov A.I., 1998, AstL, 24, 4

Lubin L.M., Bahcall, N.A., 1993, ApJ, 415, L17

Markevitch M., Sarazin C.L., Vikhlinin A., 1999, ApJ, 521, 526

McKee J.D., Mushotzky R.F., Boldt E.A., Holt S.S., Marshall F.E., Pravdo S.H., Serlemitsos P.J., 1980, ApJ, 242, 843

Mewe R., Kaastra J., Liedhal K., 1995, Legacy 6, 16

Oegerle W.R., Hill J.M., 1998, AJ, 116, 1529

Oegerle W.R., Hill J.M., 2001, ApJ, 122, 2858

Oppenheimer B.R., Helfand D.J., Gaidos E.J., 1997, AJ, 113, 2134

Parmar A.N., et al., 1997, A&AS, 122, 309

Perri M., Capalbi M., 2002, A&A, 396, 759

Postman M., Geller J.M., Huchra J.P., 1988, AJ, 95, 267

Sarazin C.L., 1988, X-ray emission from the cluster of galaxies, Cambridge University Press

Sarazin C.L., 2000, in Costructing the universe with Clusters of Galaxies, Durret F. & Gerbal D. eds., electronic proceedings http://www.iap.fr/Conferences/Colloque/coll2000/contributions

Shibata R., Honda H., Ishida M., Ohashi T., Yamashita K., 1999, ApJ, 524,603

Small T.A., Sargent W.L.W., Hamilton D., 1997, ApJS, 111, 1

Small T.A., Ma C., Sargent W.L.W., Hamilton D., 1998, ApJ, 492, 45

Struble M.F., Rood H.J., 1999, ApJS, 125, 35
Tormen G., 1997, MNRAS, 290, 411
Tormen G., Moscardini L., Yoshida N., 2004, MNRAS, 350, 1397
Venturi T., Bardelli S., Morganti R., Hunstead R.W., 2000, MNRAS, 314, 594
Wue X., Xue Y., Fang L., 1999, ApJ, 407, 470
Yee H.K.C., Ellingson E., 2003, ApJ, 585, 215
Zucca E., Zamorani G., Scaramella R., Vettolani G., 1993, ApJ, 407, 470

This paper has been typeset from a TEX/ LATEX file prepared by the author.